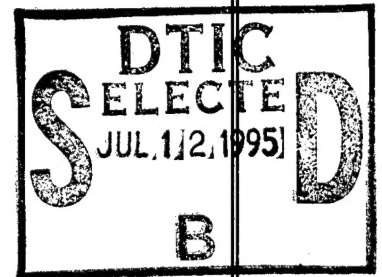


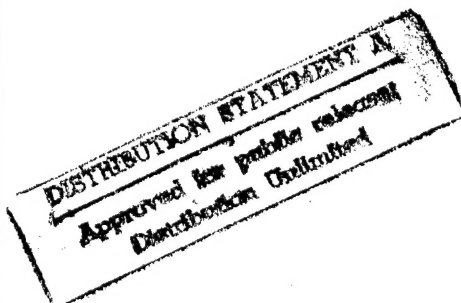
# Quarterly Technical Report

## Growth, Characterization and Device Development in Monocrystalline Diamond Films

Supported under Grant #N00014-93-I-0437  
Office of the Chief of Naval Research  
Report for the period 4/1/95-6/30/95



R. F. Davis, J. T. Glass, and R. J. Nemanich\*  
S. P. Bozeman, A. T. Sowers\* and D. Tucker  
North Carolina State University  
c/o Materials Science and Engineering Department  
\*Department of Physics  
Raleigh, NC 27695



DTIC QUALITY INSPECTED 3

June, 1995

19950703 184

5618

## REVISION NOTIFICATION

Materials Research Center  
North Carolina State University  
Raleigh, NC 27695-7919  
(919) 515-2867  
jackson@mat.mte.ncsu.edu

ADA 298/21

R. F. Davis, J. T. Glass and R. J. Nemanich

"Growth, Characterization and Device Development in Monocrystalline Diamond Films" N00014-93-I-0437

**Please replace the Report Documentation Page in our June, 1995 Quarterly Technical Report with the attached copy(ies). The abstract and subject terms have been changed.**

**(Those two sections can be pasted over the copy in the bound report.)**

# REPORT DOCUMENTATION PAGE

Form Approved  
OMB No. 0704-0188

Public reporting burden for this collection of information is estimated to average 1 hour per response, including the time for reviewing instructions, searching existing data sources, gathering and maintaining the data needed, and completing and reviewing the collection of information. Send comments regarding this burden estimate or any other aspect of this collection of information, including suggestions for reducing this burden to Washington Headquarters Services, Directorate for Information Operations and Reports, 1215 Jefferson Davis Highway, Suite 1204, Arlington, VA 22202-4302, and to the Office of Management and Budget Paperwork Reduction Project (0704-0188), Washington, DC 20503.

1. AGENCY USE ONLY (Leave blank)		2. REPORT DATE June, 1995		3. REPORT TYPE AND DATES COVERED Quarterly Technical 4/1/95-6/30/95	
4. TITLE AND SUBTITLE Growth, Characterization and Device Development in Monocrystalline Diamond Films				5. FUNDING NUMBERS s400003srr14 1114SS N00179 N66005 4B855	
6. AUTHOR(S) Robert F. Davis, J. T. Glass and R. J. Nemanich					
7. PERFORMING ORGANIZATION NAME(S) AND ADDRESS(ES) North Carolina State University Hillsborough Street Raleigh, NC 27695				8. PERFORMING ORGANIZATION REPORT NUMBER  N00014-93-I-0437	
9. SPONSORING/MONITORING AGENCY NAMES(S) AND ADDRESS(ES) Sponsoring: ONR, Code 312, 800 N. Quincy, Arlington, VA 22217-5660 Monitoring: Admin. Contracting Officer, ONR, Regional Office Atlanta 101 Marietta Tower, Suite 2805 101 Marietta Street Atlanta, GA 30323-0008				10. SPONSORING/MONITORING AGENCY REPORT NUMBER	
11. SUPPLEMENTARY NOTES					
12a. DISTRIBUTION/AVAILABILITY STATEMENT  Approved for Public Release; Distribution Unlimited				12b. DISTRIBUTION CODE	
13. ABSTRACT (Maximum 200 words)  Experimental and theoretical studies concerned with interface interactions of diamond with Si, Ni and Ni <sub>3</sub> Si substrates have been conducted. Oriented diamond films deposited on (100) Si were characterized by polar Raman, polar XRD and cross-sectional HRTEM. These studies showed that the diamond(100)/Si(100) interface adopted the 3:2-match arrangement rather than a 45°-rotation. Extended Hückel tight-binding (EHTB) electronic structure calculations for a model system revealed that the interface interaction favors the 3:2-match arrangement. Growth on polycrystalline Ni <sub>3</sub> Si resulted in oriented diamond particles; under the same growth conditions, graphite was formed on the nickel substrate. Our EHTB electronic structure calculations showed that the (111) and (100) surfaces of Ni <sub>3</sub> Si have a strong preference for diamond-nucleation over graphite-nucleation, but this was not the case for the (111) and (100) surfaces of Ni.					
14. SUBJECT TERMS diamond, silicon, Ni, Ni <sub>3</sub> Si, interface interactions, polar Raman, polar X-ray diffraction, transmission electron microscopy, Hückel tight-binding structure calculations				15. NUMBER OF PAGES 30	
				16. PRICE CODE	
17. SECURITY CLASSIFICATION OF REPORT UNCLAS	18. SECURITY CLASSIFICATION OF THIS PAGE UNCLAS	19. SECURITY CLASSIFICATION OF ABSTRACT UNCLAS	20. LIMITATION OF ABSTRACT SAR		

## Table of Contents

I.	Introduction	1
II.	Comparison of Silicon, Nickel and Nickel Silicide ( $\text{Ni}_3\text{Si}$ ) as Substrates for Epitaxial Diamond Growth	2
III.	Distribution List	30

Accession For	
NTIS GRA&I	<input checked="" type="checkbox"/>
DTIC TAB	<input type="checkbox"/>
Unannounced	<input type="checkbox"/>
Justification	
By	
Distribution/	
Availability Codes	
Dist	Avail and/or Special
A-1	

## I. Introduction

Diamond as a semiconductor in high-frequency, high-power transistors has unique advantages and disadvantages. Two advantages of diamond over other semiconductors used for these devices are its high thermal conductivity and high electric-field breakdown. The high thermal conductivity allows for higher power dissipation over similar devices made in Si or GaAs, and the higher electric field breakdown makes possible the production of substantially higher power, higher frequency devices than can be made with other commonly-used semiconductors.

In general, the use of bulk crystals severely limits the potential semiconductor applications of diamond. Among several problems typical for this approach are the difficulty of doping the bulk crystals, device integration problems, high cost and low area of such substrates. In principal, these problems can be alleviated via the availability of chemically vapor deposited (CVD) diamond films. Recent studies have shown that CVD diamond films have thermally activated conductivity with activation energies similar to crystalline diamonds with comparable doping levels. Acceptor doping via the gas phase is also possible during activated CVD growth by the addition of diborane to the primary gas stream.

The recently developed activated CVD methods have made feasible the growth of polycrystalline diamond thin films on many non-diamond substrates and the growth of single crystal thin films on diamond substrates. More specifically, single crystal epitaxial films have been grown on the {100} faces of natural and high pressure/high temperature synthetic crystals. Crystallographic perfection of these homoepitaxial films is comparable to that of natural diamond crystals. However, routes to the achievement of rapid nucleation on foreign substrates and heteroepitaxy on one or more of these substrates has proven more difficult to achieve. This area of study has been a principal focus of the research of this contract.

At present, the feasibility of diamond electronics has been demonstrated with several simple experimental devices, while the development of a true diamond-based semiconductor materials technology has several barriers which a host of investigators are struggling to surmount. It is in this latter regime of investigation that the research described in this report has and continues to address.

In this reporting period, experimental and theoretical studies concerned with interface interactions of diamond with Si, Ni and Ni<sub>3</sub>Si substrates have been conducted. Oriented diamond films deposited on (100) Si were characterized by polar Raman, polar XRD and cross-sectional HRTEM. Growth on polycrystalline Ni<sub>3</sub>Si resulted in oriented diamond particles; under the same growth conditions, graphite was formed on the nickel substrate. Extended Hückel tight-binding (EHTB) electronic structure calculations for a model system were also conducted.

## II. Comparison of Silicon, Nickel and Nickel Silicide ( $\text{Ni}_3\text{Si}$ ) as Substrates for Epitaxial Diamond Growth

D. A. Tucker (a), D.-K. Seo (b), M.-H. Whangbo (b), F. R. Sivazlian (a), B. R. Stoner (d), S. P. Bozeman (a), A. T. Sowers (c), R. J. Nemanich (c), and J. T. Glass (d)

(a) Department of Materials Science and Engineering, North Carolina State University, North Carolina 27695-7919

(b) Department of Chemistry, North Carolina State University, North Carolina 27695-8204

(c) Department of Physics, North Carolina State University, North Carolina 27695-8202

(d) Kobe Steel USA Inc., Electronic Materials Center, 79 T. W. Alexander Drive, PO Box 13608, Research Triangle Park, North Carolina 27709

### Abstract

We carried out experimental and theoretical studies aimed at probing interface interactions of diamond with Si, Ni and  $\text{Ni}_3\text{Si}$  substrates. Oriented diamond films deposited on (100) silicon were characterized by polar Raman, polar XRD and cross-sectional HRTEM. These studies show that the (100)-diamond/(100)-Si interface does not adopt the  $45^\circ$ -rotation but the 3:2-match arrangement. Our extended Hückel tight-binding (EHTB) electronic structure calculations for a model system show that the interface interaction favors the 3:2-match arrangement. Growth on polycrystalline  $\text{Ni}_3\text{Si}$  resulted in oriented diamond particles while, under the same growth conditions, largely graphite was formed on the nickel substrate. Our EHTB electronic structure calculations for model systems show that the (111) and (100) surfaces of  $\text{Ni}_3\text{Si}$  have a strong preference for diamond-nucleation over graphite-nucleation, but this is not the case for the (111) and (100) surfaces of Ni.

## A. Introduction

Diamond has many excellent properties (e.g., large bandgap, high hole mobility, optical transparency, large thermal conductivity, chemical inertness, and high hardness) that are important for applications in high temperature electronic devices, tool coatings, heat sinks, and optical windows. For the microelectronics industry to capture the full utility of diamond's unique properties, however, it is necessary to attain heteroepitaxial diamond. Currently, thin film growth of single crystal diamond has not been achieved, and the chemistry involved in diamond nucleation on a substrate surface is poorly understood. Studies of diamond nucleation and interfaces can help improve adhesion, control morphology, and produce heteroepitaxy. All these aspects are important in applications of diamond thin-films for electronic purposes, wear and optical coatings.

At present, there is no completely lattice-matched substrate for heteroepitaxial diamond growth, but several have a relatively small lattice mismatch: cubic boron nitride (1.5 %), nickel (1.2 %), copper (1.2 %), and cobalt (0.6 %). Currently, oriented diamond particles have been deposited on cubic boron nitride (cBN) [1-4], silicon [5-7], silicon carbide [8-10], nickel [11-15], cobalt [16], beryllium oxide [17], and graphite [18,19] by different growth methods (e.g., DC plasma, microwave, and hot-filament), and novel processes utilizing these methods have been employed to produce these oriented diamond particles (e.g., the bias-enhanced nucleation process developed by Stoner *et al.* [5,20,21] and the seeding-annealing-growth process developed by Yang *et al.* [12-15]). However, all of these substrates possess some limitations: For example, cBN is attractive in terms of the small lattice mismatch and the expected interface chemical bonding (e.g., C-N and C-B bond formation), but it is very difficult to produce single crystals of cBN suitable in size for substrates. Stoner *et al.* [5,8,9] obtained oriented diamond particles on silicon and silicon carbide ( $\beta$ -SiC) by the bias-enhanced nucleation process, but the large lattice mismatch (34% for Si and 18% for  $\beta$ -SiC) leads to misorientation in the resulting diamond particles. In diamond growth on silicon, the percentage of oriented particles (with respect to the substrate lattice) after the bias-nucleation step can be as high as 50 %. From these particles, highly oriented films, in which nearly all of the grains are aligned to within about  $6^\circ$  of the substrate, can be grown [5,7] by a judicious use of the van der Drift evolutionary method [22]. Normal diamond growth conditions on nickel and cobalt substrates usually result in graphite or graphite interlayers [23,24]. However, oriented diamond particles can be grown on these substrates by using the process of Yang *et al.* [12-15], which consists of seeding the metal surface with carbon powders (either diamond or graphite), annealing the sprinkled powders in a high temperature step, and growing diamond particles on the annealed surface under typical diamond growth conditions. It is believed that the annealing step produces a supersaturated M-C-H (M = Ni or Co) phase on the substrate surface, and diamond nucleation starts from this phase upon assuming the typical diamond growth conditions. Nickel and cobalt

have a relatively close lattice match with diamond (1.2 and 0.6 % mismatch, respectively). However, it is difficult to obtain complete diamond films probably because the carbon continues to dissolve into the substrate during growth, as evidenced by lack of stable carbide formation. In the search for a suitable substrate for improved heteroepitaxial diamond growth, therefore, the lattice-matching and strong directional bond formation in the diamond/substrate interface appear to be essential.

Several theoretical studies examined interface interactions in (100)-diamond/(100)-Si, (100)-diamond/(100)-Ni, and (111)-diamond/(111)-Ni. On the basis of MNDO and PM3 semiempirical SCF-MO calculations, Verwoerd examined the (100)-diamond/(100)-Si interface [25-28]. To reduce the large lattice mismatch (34%), he first considered an arrangement in which one (100) surface is rotated by  $45^\circ$  with respect to the other (hereafter, referred to as the  $45^\circ$ -rotation arrangement) since it provides a much smaller lattice mismatch (7%) [25,26]. As an alternative arrangement for the (100)-diamond/(100)-Si interface, Verwoerd considered the possibility that the epitaxy arises from matching three diamond unit cells to two silicon unit cells without rotating the two surfaces (hereafter, referred to as the 3:2-match arrangement) [27,28]. The lattice constants of the Si/diamond (100) surfaces have a ratio very close to 3:2, and the lattice mismatch is only 1.5 % from this viewpoint. In Verwoerd's calculations, the positions of the surface and subsurface atoms are completely relaxed, and the atoms of one surface are allowed to penetrate into the lattice of the other surface. His calculations suggest that the 3:2-match arrangement becomes energetically favored over the  $45^\circ$ -rotated arrangement when the diamond overlayer is thick enough (greater than 3 atomic layers) [27,28]. Pickett and Erwin studied the (100)-diamond/(100)-Ni and (111)-diamond/(111)-Ni interfaces on the basis of ab initio electronic band structure calculations [29-35]. For each interface they considered two arrangements: one emphasized the "tetrahedral bonding" by placing the carbon atoms at the bridge positions of the (100) Ni surface and at the atop positions of the (111) Ni surface. The other arrangement maximized "metallic bonding" by placing the carbon atoms at the missing Ni positions above the Ni surface, which are 4-fold hollow sites of the (100) Ni surface and 2-fold hollow sites of the (111) Ni surface. For both (100)-diamond/(100)-Ni and (111)-diamond/(111)-Ni interfaces, the "tetrahedral bonding" arrangement was calculated to be more favorable [31].

In the present work, we carry out both experimental and theoretical studies aimed at probing interface interactions of diamond with Si, Ni and  $\text{Ni}_3\text{Si}$  substrates. The nickel silicide  $\text{Ni}_3\text{Si}$  has the  $\text{Cu}_3\text{Au}$ -type structure, and its (100) surface ( $3.504 \text{ \AA}$ ) has a small lattice mismatch with the (100) diamond surface (1.8 %). Silicon readily forms a stable carbide, whereas nickel carbide is metastable. As mentioned above, under normal diamond growth conditions, nucleation attempts on Ni usually results in graphite, while that on Si leads to diamond particles. Thus, for  $\text{Ni}_3\text{Si}$ , one might expect that the Si atoms make interface bonds

with the diamond carbon atoms, and the small lattice mismatch reduces the misorientation of the diamond particles. To help explain our experimental observations of diamond and/or graphite growth on Si, Ni and Ni<sub>3</sub>Si substrates, we examine their associated interface interactions on the basis of extended Hückel tight-binding (EHTB) electronic band structure calculations [36].

## B. Experimental

*Growth on Silicon.* Diamond films were deposited on (100) silicon substrates utilizing a microwave plasma chemical vapor deposition (CVD) reactor (AS<sup>Te</sup>X™). A more detailed description is given elsewhere [21]. Silicon wafers were cleaned by dipping into a dilute hydrofluoric acid for one minute, rinsed with deionized water before loading into the chamber, and then subjected to a three-step growth process (i.e., carburization, nucleation and thin-film growth) similar to what has been described previously [6]. In the nucleation step, which lasts approximately 3–10 minutes, the substrate is biased at -250 V while immersed in the methane/hydrogen plasma. Finally, from the resulting oriented nuclei, typical deposition conditions are used to grow diamond films. The diamond films were characterized by Raman spectroscopy, scanning electron microscopy (SEM), X-ray diffraction (XRD), and high resolution transmission electron microscopy (HRTEM).

Most of these techniques have been frequently used in characterization of diamond films. Polar XRD is especially effective at determining texture, orientation and crystallographic quality of films [37-39]. Although polarization sensitive Raman spectroscopy (PSR) is not as popular, it can be successfully used to give crystallographic information [3,4,40].

Raman spectroscopy has established itself as a key technique for determining the quality of diamond thin films. The basic application of Raman scattering is to evaluate the sp<sup>2</sup>/sp<sup>3</sup> bonding ratio and strain present in the films. However, due to anisotropy in the Raman scattering tensor for the diamond crystal structure [41], Raman spectroscopy can also be used to characterize the crystallographic orientation of highly oriented or single crystal diamond samples. In these polar Raman measurements the observed Raman scattering intensity is function of the incident laser beam polarization, the sample orientation, and the polarization of the observed scattered light.

For the crystallographic measurements the routine Raman scattering apparatus is used with slight modifications. The incident laser beam is polarized vertically using a polarization rotator/linear polarizer combination. The sample is mounted on a rotary stage and the axis of rotation is normal to the sample surface. The Raman scattered light is collected and passed through another linear polarizer with its transmission axis vertically oriented before entering the monochromator.

With the scattering apparatus in this configuration, the sample stage is rotated through  $360^\circ$  in  $10^\circ$  increments. At each increment Raman spectra of the silicon and diamond peaks ( $520\text{ cm}^{-1}$  and  $1332\text{ cm}^{-1}$ , respectively) are taken. The polar response for both silicon and diamond is then obtained by plotting the scattering intensity of each peak versus the sample rotation angle.

*Growth on  $\text{Ni}_3\text{Si}$  and Ni.* The deposits on  $\text{Ni}_3\text{Si}$  and Ni substrates were both grown and analyzed in the in-vacuo CVD and surface analysis apparatus (Fig. 1), which consists of a hot-filament CVD (HFCVD) system connected to two analytical chambers via a transfer station. Once the substrates are introduced into the apparatus, however, the samples can be transferred into the analysis chamber without exposure to atmosphere. The HFCVD chamber is a modified six-way cross processed by a dual-stage rotary pump during diamond deposition. Filaments utilized in diamond growth were spiral tungsten filaments powered by a Sorensen DC power supply. One chamber is equipped with an X-ray source (dual anode VG XR3E2) for X-ray photoelectron spectroscopy (XPS), an electron gun (VG LEG62) for Auger electron spectroscopy (AES), and a hemispherical electron energy analyzer (VG CLAM II). Another chamber is outfitted with an ion gun used to clean the substrates. The two chambers are

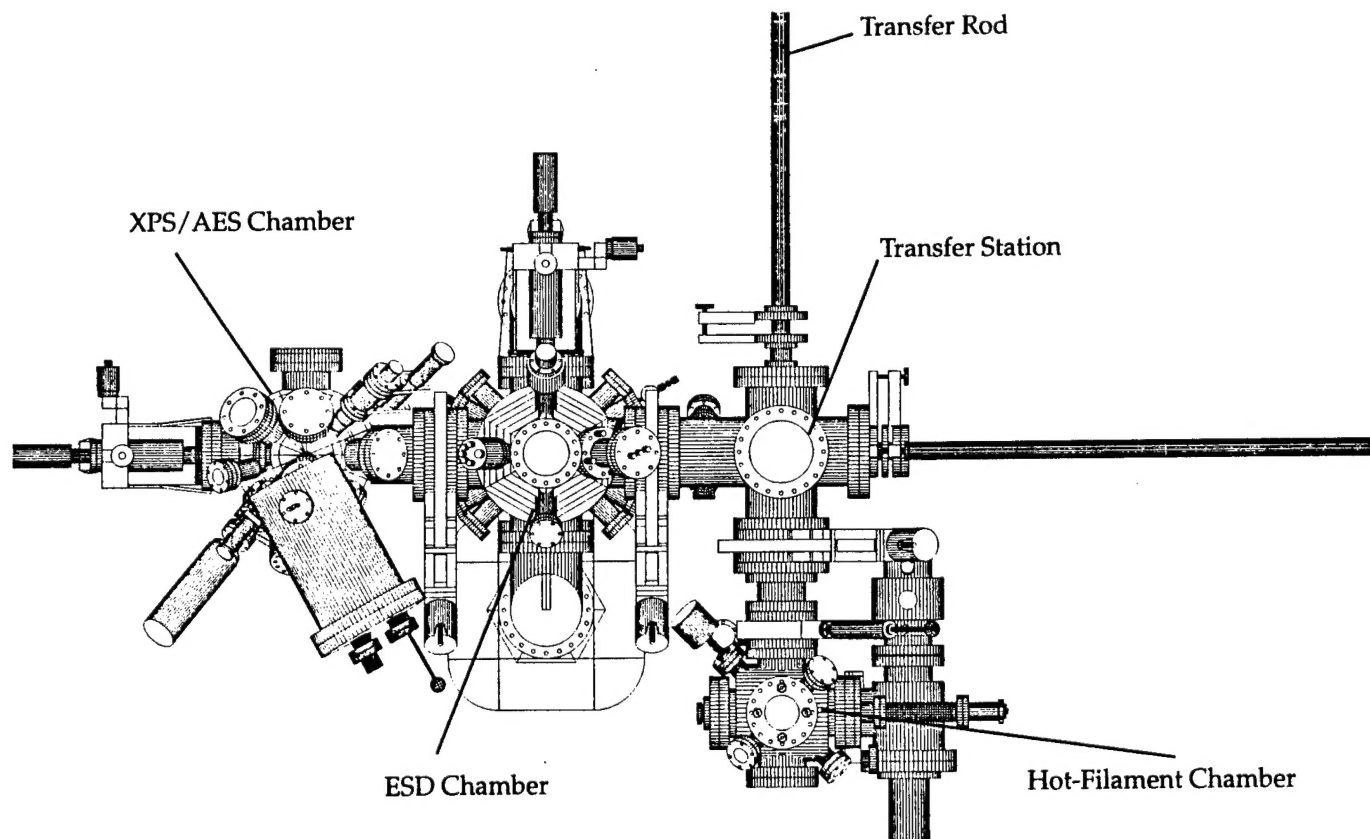


Figure 1. Schematic diagram of growth and surface-characterization systems. ESD refers to electron stimulated desorption.

pumped by an ion pump (Perkin Elmer 400 l/s) and a water-cooled titanium sublimation pump. A base pressure for the two chambers (typically  $3 \times 10^{-10}$  Torr) was monitored by an ionization gauge. XPS and AES spectra, both collected in pulse-counting mode, were acquired with a software package (VGX900). In addition, the AES spectra were differentiated with this software.

Ni<sub>3</sub>Si was produced by an arc melting and drop casting technique from a stoichiometric mixture of Ni and Si (by Dr. C. T. Liu and coworkers, Metals and Ceramics Division, Oak Ridge National Laboratory). The resulting silicide was characterized by metallography, XRD (both diffractometer and Debye-Scherrer), XPS, and AES. Diamond films were deposited on Ni<sub>3</sub>Si in the HFCVD chamber described earlier. The same conditions were used in depositing on polycrystalline Ni for the purpose of comparisons. Both the Ni<sub>3</sub>Si and Si substrates were polished (down to 0.01  $\mu$ m alumina) before deposition. Typical experimental conditions were: a filament temperature of over 2200°C, substrate temperature of approximately 850°C, pressure of 20 Torr, and methane concentration of 1 % in hydrogen. The films deposited on the Ni<sub>3</sub>Si and Ni substrates were characterized by SEM, Raman spectroscopy, XPS and AES.

### C. Experimental Results

*Growth on Silicon.* The diamond films grown on (100) silicon were both highly oriented and textured to within 10° of the (100) Si. The SEM micrograph of a typical diamond film is shown in Fig. 2. Figure 3 displays a progression of the SEM micrographs, polarization sensitive Raman spectra (PSR), and polar XRD spectra as a function of the thickness of the grown diamond layer. In the Raman spectra, the solid and open circles refer to the silicon and diamond responses, respectively (both have been normalized). The improvement of texturing, visually detected from the SEM micrographs (Fig. 3a), is verified in the polar XRD patterns (Fig. 3c): the {220} twin spots disappear at higher thicknesses, and the area of the {220} spots decreases progressively. The {220} spots for the thicker film are asymmetric with a FWHM of 10° and 8° in the radial and transversal directions, respectively. The FWHM relates to a minor misorientation of the particles and corresponds to a tilt of the diamond out of the (100) surface plane and an azimuthal rotation of the diamond in the plane. The polarization sensitive Raman spectra (Fig. 3b) also confirm the improvement in orientation with texturing: with increasing thickness, the response of the diamond film becomes more similar to that of the cloverleaf pattern of the underlying silicon. This occurs because both diamond and silicon have the same crystal structure and thus have the same surface theoretical dependence on rotation. This phenomenon is described by the equation  $I \propto \sin^2(2\theta)$ , where  $I$  is the intensity of the Raman vibration and  $\theta$  is the rotation angle of the sample. These Raman spectra strongly suggest that the diamond is predominantly aligned with respect to the (001) Si planes and [110] directions, i.e., there is no evidence of a 45°-rotation of the diamond atop the silicon in the

(100)-diamond/(100)-Si interface. If this rotation were present, the "cloverleaf" pattern of the diamond response would be rotated from that of the silicon response by  $45^\circ$ .

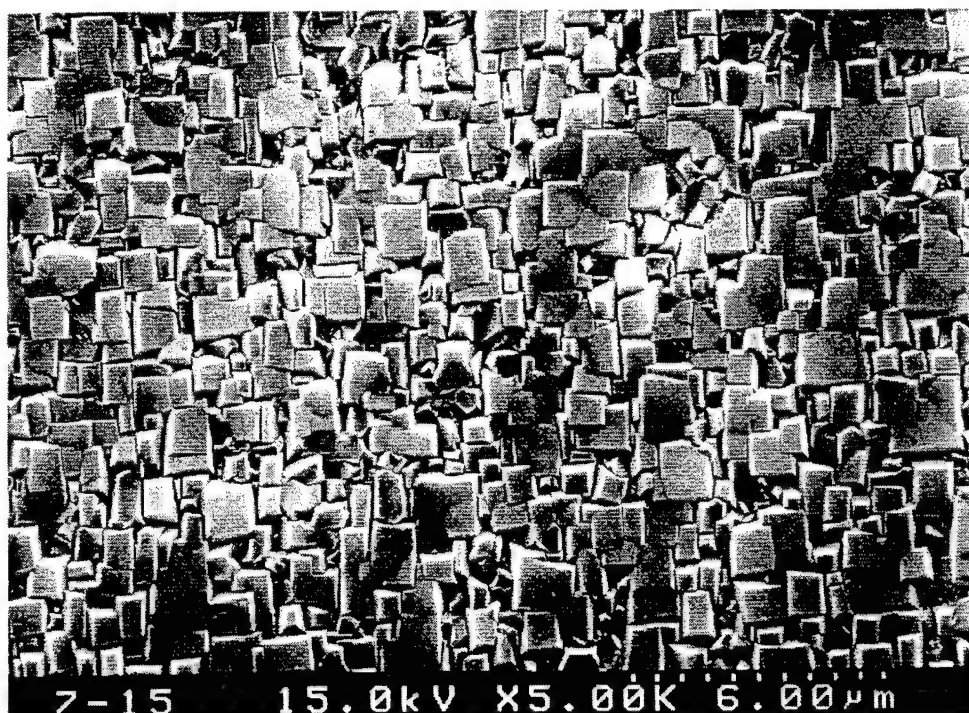


Figure 2. SEM micrograph of a textured diamond film grown on a (100) silicon substrate by the three-step process, which consists of the carburization, the bias-enhanced nucleation and the textured-growth steps.

The intent of the carburization step in the experimental procedure was to form a silicon carbide interlayer, because a HRTEM study has shown evidence for oriented diamond on  $\beta$ -SiC [10]. A cross-sectional HRTEM micrograph taken for a diamond particle grown on a (100) Si surface is presented in Fig. 4, where the parallel linear patterns originate from the atoms of the (111) planes of the diamond and silicon lattice. The HRTEM micrograph shows what appears to be an epitaxial interface in which diamond is oriented on the silicon without a visible silicon carbide interlayer. Also a selected area diffraction pattern of the interface exhibits no spots characteristic of silicon carbide. Thus, the formation of an observable  $\beta$ -SiC interlayer does not appear necessary in growing diamond on the (100) Si surface. (However, other areas of the same sample do show the presence of a silicon carbide interlayer.) As schematically depicted in Fig. 5, the HRTEM micrograph suggests that the ratio of the diamond (111) planes to the silicon (111) planes is close to 3:2, and there occurs an approximately  $9^\circ$  tilt of the (111) diamond planes out of the (100) surface. We note that a  $9.5^\circ$  tilting is needed for the diamond

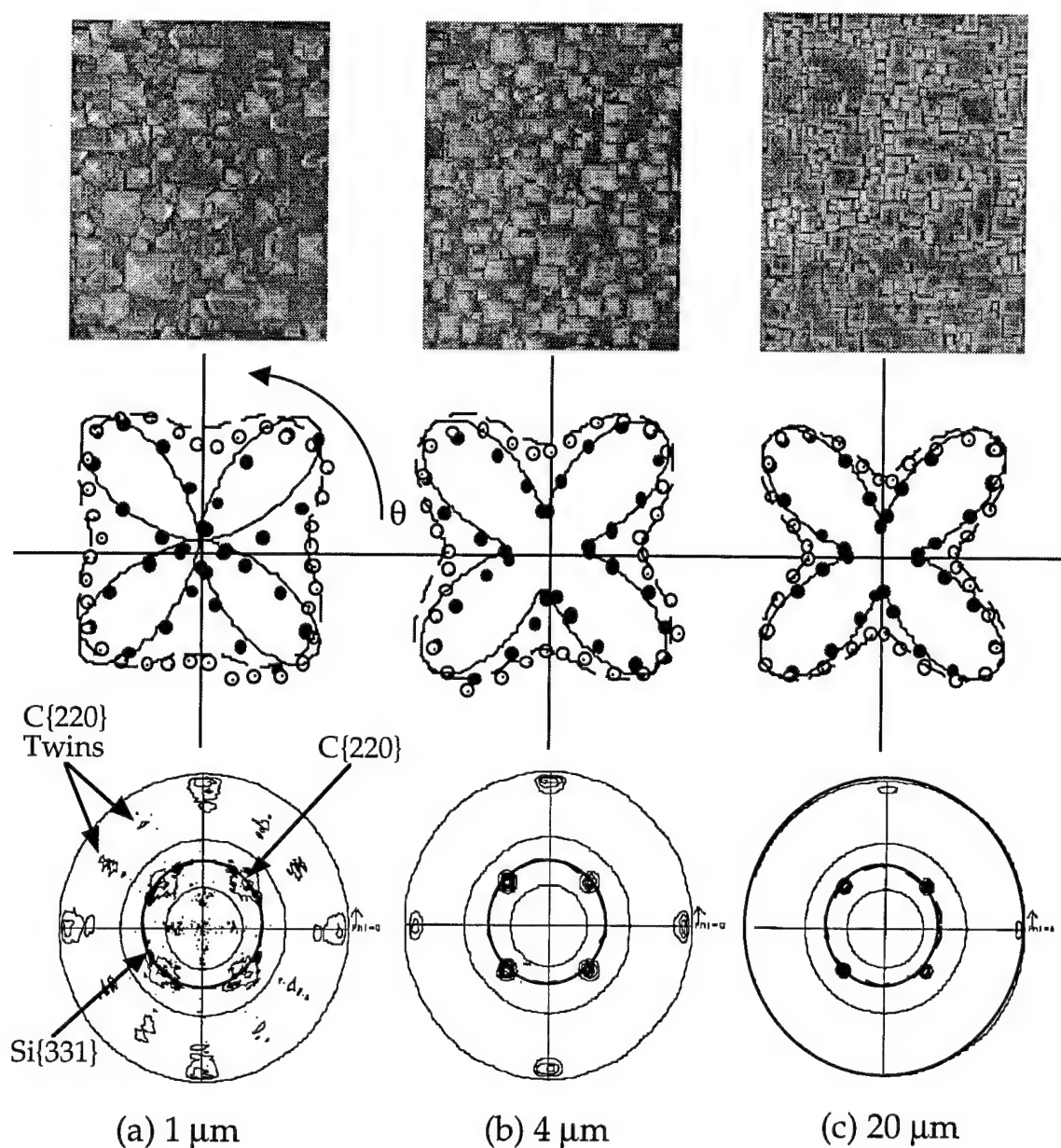


Figure 3. SEM micrographs (top), polar Raman spectra (middle) and polar XRD spectra (bottom) taken for the diamond growth on (100) Si for diamond-film thicknesses of (a) 1  $\mu\text{m}$ , (b) 4  $\mu\text{m}$  and (c) 20  $\mu\text{m}$ . The open and filled circles of the polar Raman spectra refer to the diamond film and the Si substrate, respectively. The  $\{220\}$  spots of the polar XRD spectrum in Figure 3c are asymmetric with a FWHM in the radial and transversal directions of  $10^\circ$  and  $8^\circ$ , respectively. This indicates that the texturing reduces the extent of tilting, but not that of azimuthal misorientation. This observation is consistent with the van der Drift method.

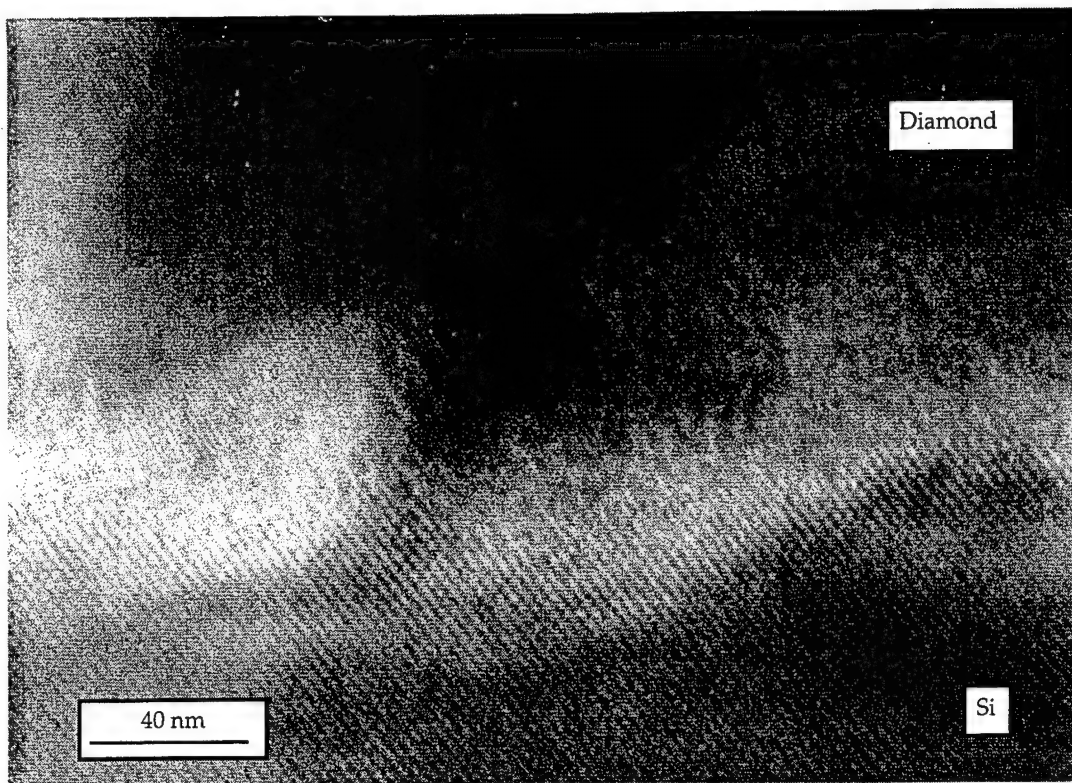


Figure 4. Cross-sectional HRTEM micrograph taken for an oriented diamond/silicon interface.

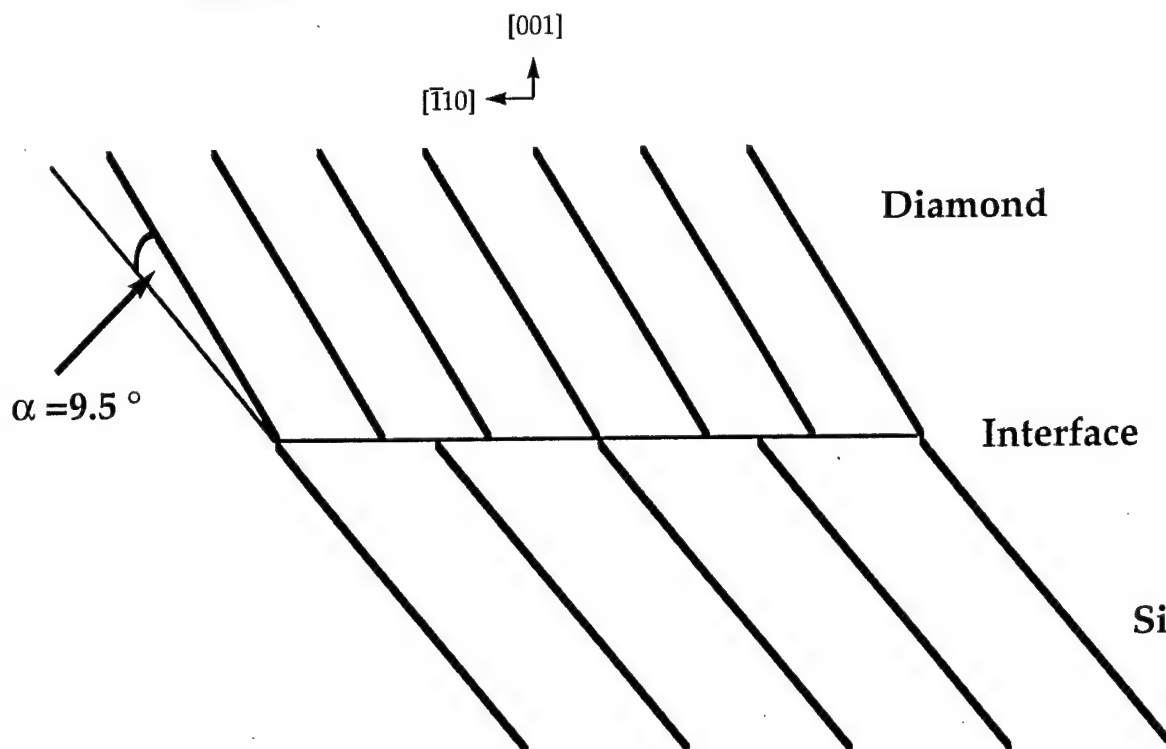


Figure 5. Schematic representation of the cross-sectional HRTEM micrograph predicted for the (100)-diamond/(100)-Si interface under the assumption that the interface adopts the 3:2-match arrangement, and the 1.5 % mismatch results in a tilt of the (111) diamond planes by  $\alpha = 9.5^\circ$ .  $\alpha = \arccos(3a_{\text{diamond}}/2a_{\text{Si}})$ , where  $a_{\text{diamond}}$  and  $a_{\text{Si}}$  are the lattice constants for diamond and Si, respectively.

and silicon lattices to match perfectly with a 3:2 registry of the planes. In addition, the HRTEM micrographs observed in this study do not reveal evidence of a 45°-rotation of the diamond atop the silicon surface in the (100)-diamond/(100)-Si interface. If this rotation were present, the HRTEM micrograph would not show the (111) planes of both diamond and silicon.

*Growth on Ni<sub>3</sub>Si and Ni*. Quantitative XPS and AES analyses of Ni<sub>3</sub>Si samples show that the Ni/Si composition ratio is close to 3, as expected. However, our XRD and optical microscopy measurements show that the Ni<sub>3</sub>Si samples contain more than one phase. An optical micrograph of the Ni<sub>3</sub>Si sample after a grain boundary etch is presented in Fig. 6. The Ni<sub>3</sub>Si sample is polycrystalline with an average grain size of approximately 20 μm in diameter and consists of two phases (labeled as 1 and 2 in Figure 6). Figure 7 compares the observed XRD diffraction pattern of Ni<sub>3</sub>Si (black lines) with the JCPDS (Joint Committee on Powder Diffraction Standards) pattern of cubic Ni<sub>3</sub>Si (gray lines). The observed peaks match well with the JCPDS pattern of cubic Ni<sub>3</sub>Si, except for the two peaks at 2θ = 46.0° and 47.3°, which are consistent with the high temperature monoclinic Ni<sub>3</sub>Si phase. This phase can be annealed out of the samples at high temperatures.

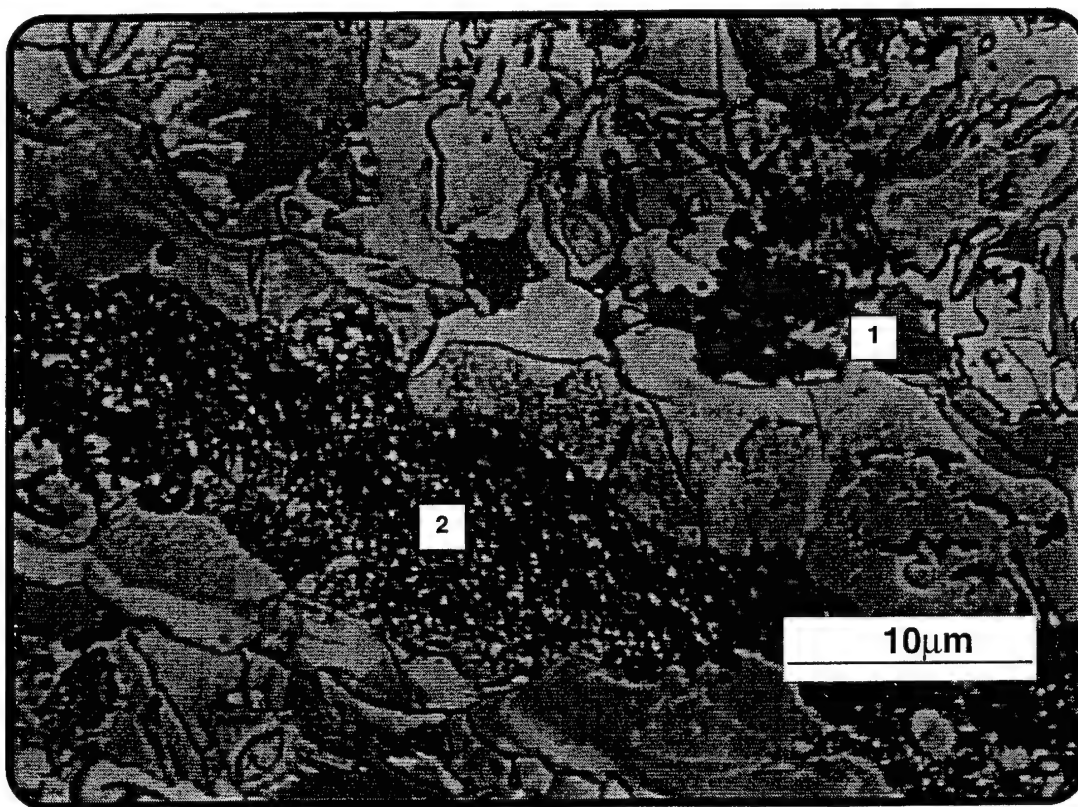


Figure 6. Optical micrograph of a bulk Ni<sub>3</sub>Si sample at 500X. The sample was polished down to 0.01 μm alumina and then subjected to a 10 min grain boundary etching.

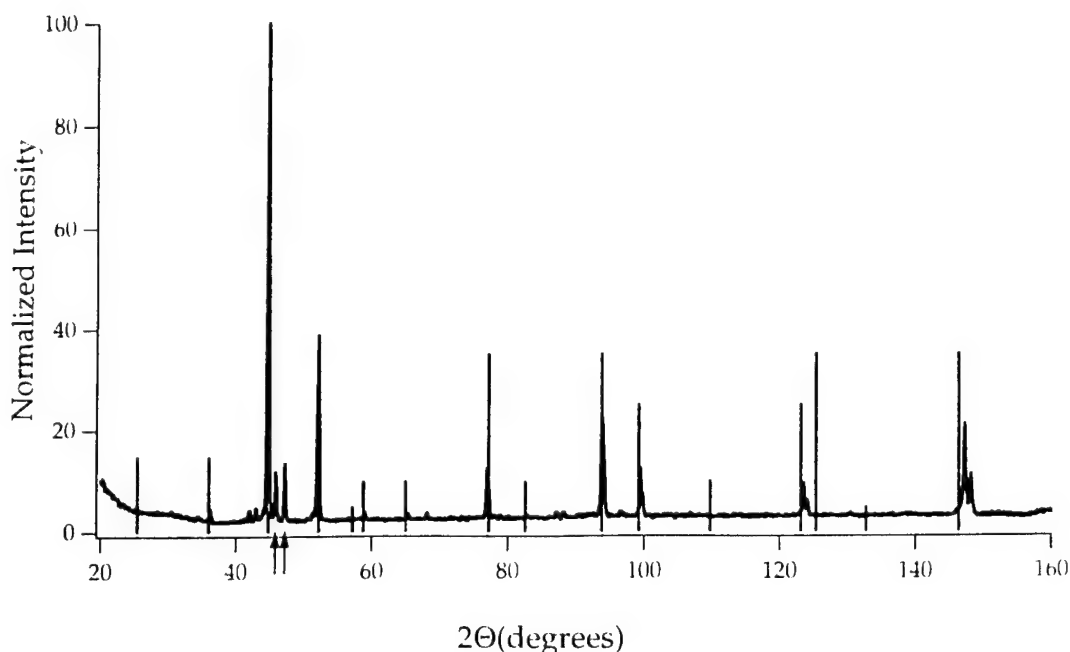


Figure 7. XRD pattern of the  $\text{Ni}_3\text{Si}$  sample in black, which was overlaid with the JCPDS pattern for cubic  $\text{Ni}_3\text{Si}$  in gray. The two peaks indicated by arrows are consistent with the high temperature, monoclinic  $\text{Ni}_3\text{Si}$  phase.

The diamond particles resulting from growth on cubic  $\text{Ni}_3\text{Si}$  are presented in the two SEM micrographs of Fig. 8, which show well-faceted, oriented diamond particles on  $\text{Ni}_3\text{Si}$ , presumably within a single grain. Shown in Fig. 9 are two SEM micrographs of the growth on Ni. The majority of the growth on Ni is graphitic (Fig. 9a), but poorly faceted particles are also found (Fig. 9b). The micro-Raman spectra for the growth on  $\text{Ni}_3\text{Si}$  and Ni are presented in Figs. 10a and 10b, respectively. For the growth on  $\text{Ni}_3\text{Si}$  the spectrum shows a sharp peak centered at  $1332\text{ cm}^{-1}$  with a FWHM of  $3.6\text{ cm}^{-1}$ , which signifies high quality diamond. For the growth on Ni, however, the spectrum exhibits a fairly weak/broad peak centered at approximately  $1350\text{ cm}^{-1}$  and a large/broad peak at  $1580\text{ cm}^{-1}$ . These findings show that the growth on Ni is a mixture of amorphous carbon and graphite [42], while well-faceted and possibly oriented diamond particles could be attained on  $\text{Ni}_3\text{Si}$ .

#### D. Estimation of Interface Interactions

*Growth on Si.* In general, the existence of a large lattice mismatch between a substrate and overgrowth prevents epitaxy, so it is surprising that oriented (100) diamond particles are grown on (100) silicon despite the large mismatch between diamond and silicon (34 %). The present TEM, PSR and polar XRD studies show that the  $45^\circ$ -rotation is absent in the (100)-diamond/(100)-Si interface. We now examine the interface interactions associated with the  $45^\circ$ -rotation and 3:2-match arrangements by performing EHTB electronic band structure calculations on suitable model systems. Verwoerd's calculations [27,28] showed that

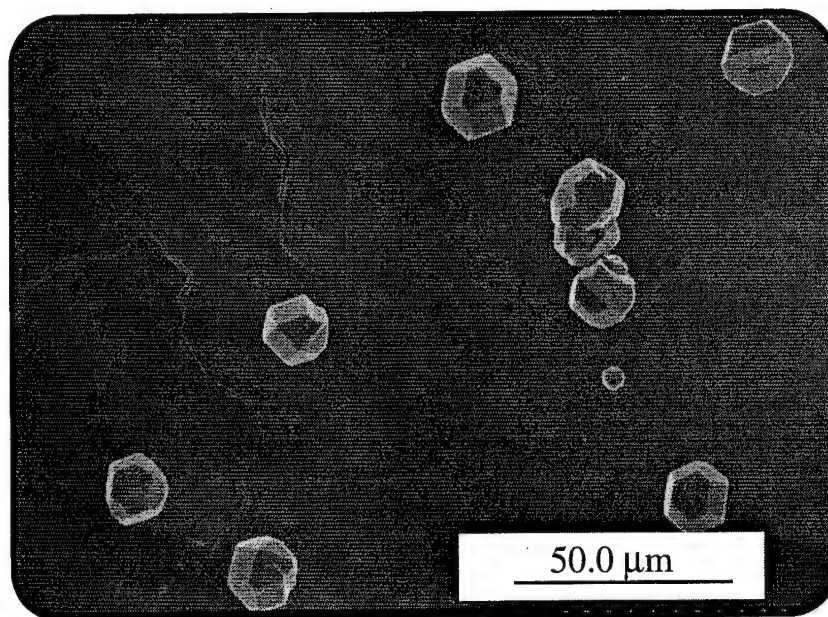
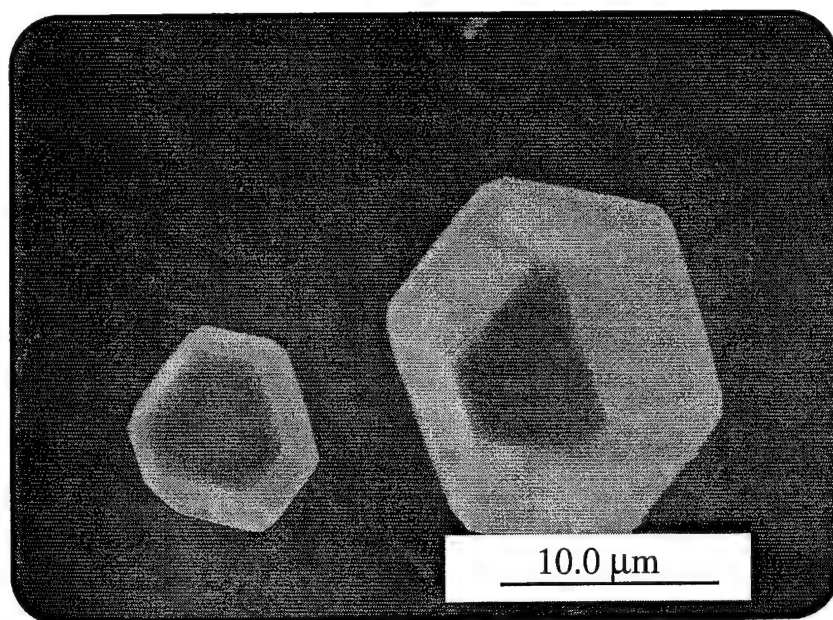
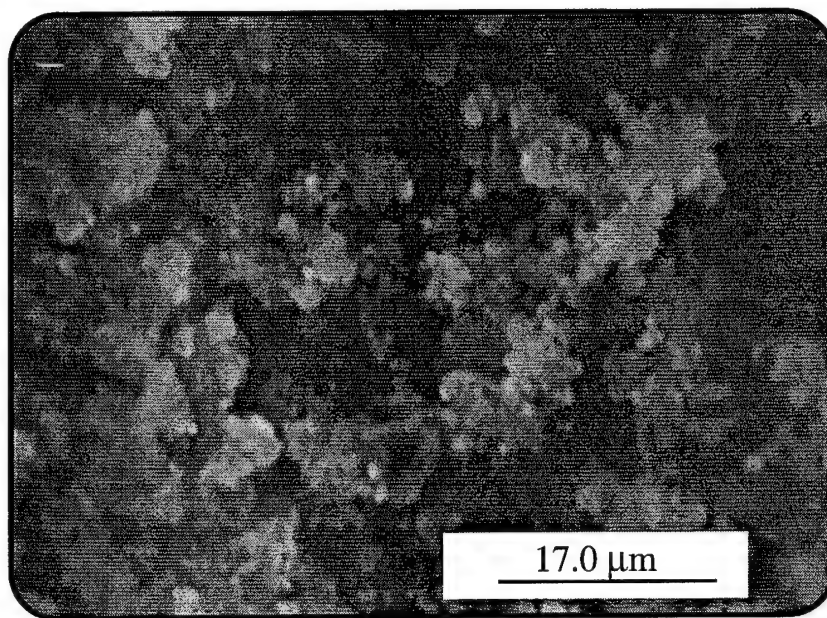
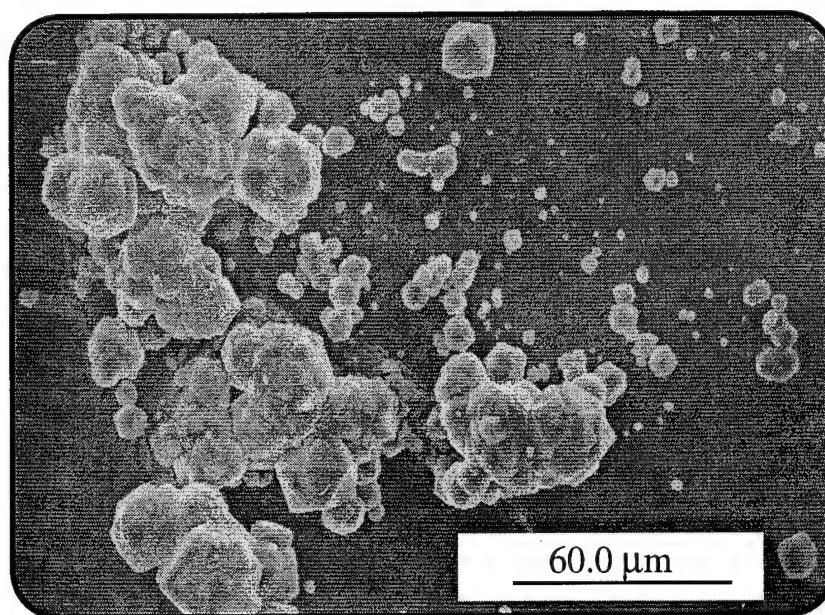


Figure 8. SEM micrographs of diamond particles deposited on  $\text{Ni}_3\text{Si}$  after 16 hours growth under conditions of 1 %  $\text{CH}_4/\text{H}_2$  and substrate temperature of  $850^\circ\text{C}$ . Parallel lines on the micrographs mark particles that seem to be oriented.

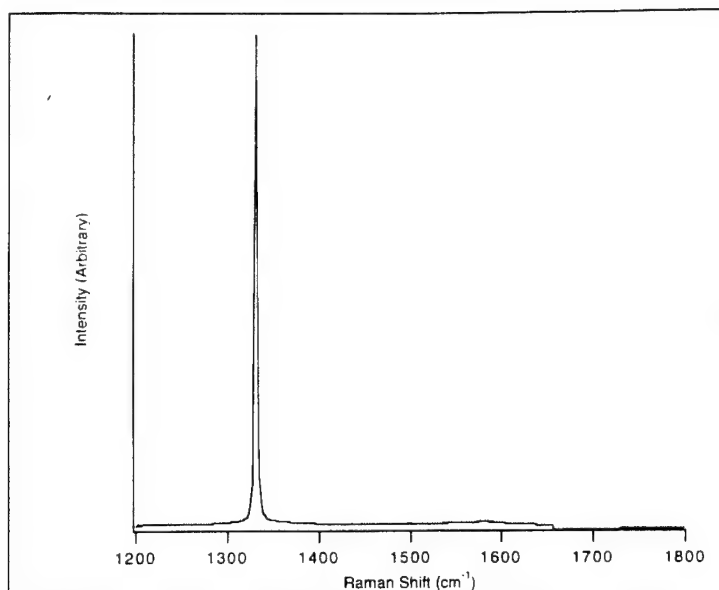


**a**

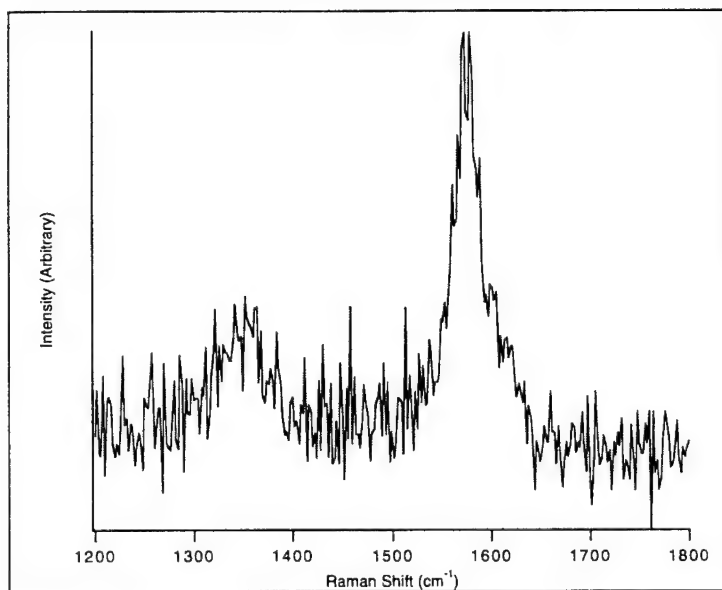


**b**

Figure 9. SEM micrographs of growths on Ni under the same conditions as used for the diamond growth on  $\text{Ni}_3\text{Si}$ . The majority of the substrate is covered by graphite in (a), and some of the substrate has poorly faceted diamond deposits in (b).



a



b

Figure 10. Micro-Raman spectra of (a) a diamond particle grown on  $\text{Ni}_3\text{Si}$  and (b) a graphite growth on Ni. The sharp peak at  $1332\text{ cm}^{-1}$  (FWHM of  $3.6\text{ cm}^{-1}$ ) of Fig. 11a signifies high quality diamond. The broad peaks at  $1350$  and  $1580\text{ cm}^{-1}$  of Fig. 11b suggest that the growth is a mixture of graphite and amorphous carbon.

strain energy is a crucial part of the energetics in determining the interface interaction energies. To carry out realistic calculations of interface interaction energies, the positions of the surface and subsurface atoms are completely relaxed. Since the extended Hückel method is inadequate for bond length optimization, we ignore the elastic deformation in the heteroepitaxial layers in our EHTB calculations for the interface interaction energies associated with the  $45^\circ$ -rotation and 3:2-match arrangements.

The interface interactions are simulated by placing  $C_7$  diamond clusters (Fig. 11) on a 3-layer silicon slab (Fig. 12). Except for two dangling bonds for each of the four carbon atoms at the bottom surface of the  $C_7$  cluster, all dangling bonds of the  $C_7$  cluster were capped with

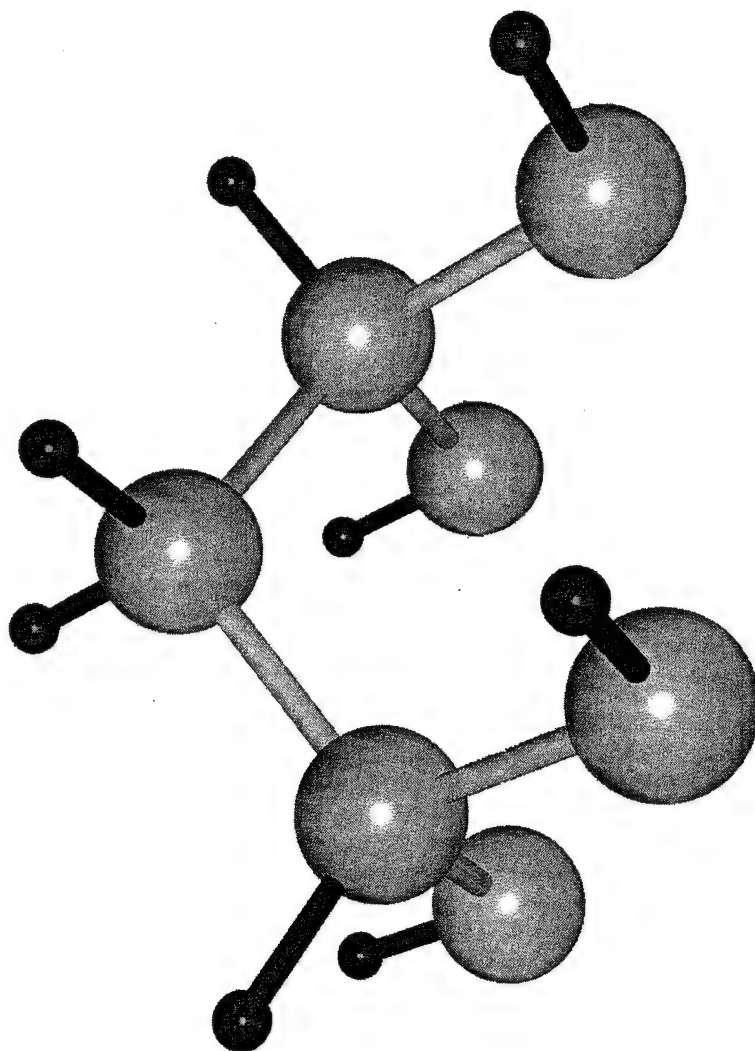
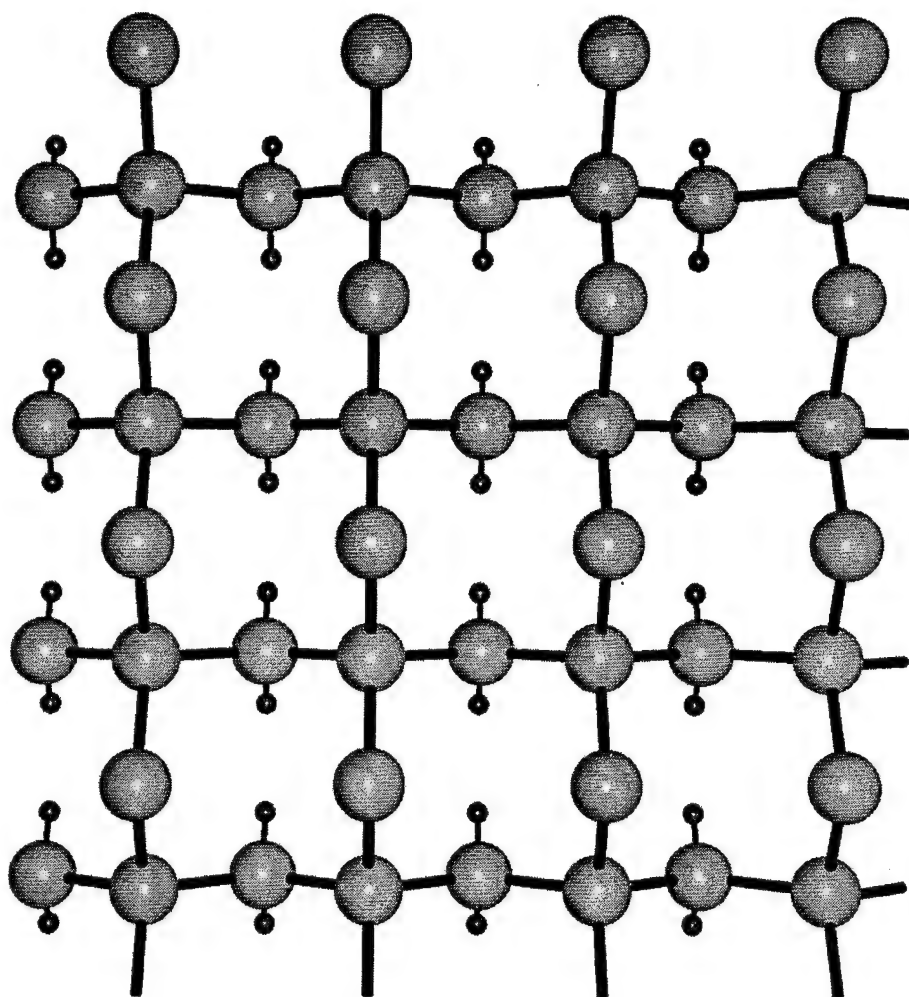
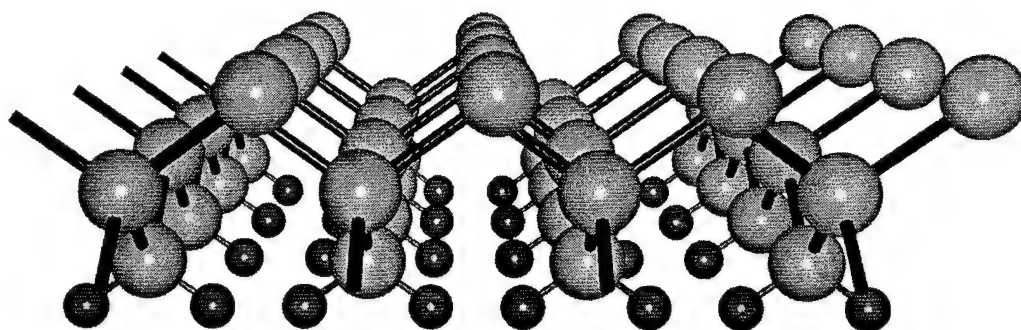


Figure 11. Perspective view of the  $C_7$  diamond cluster employed for the study of the (100)-diamond/(100)-Si interface interaction.



a



b

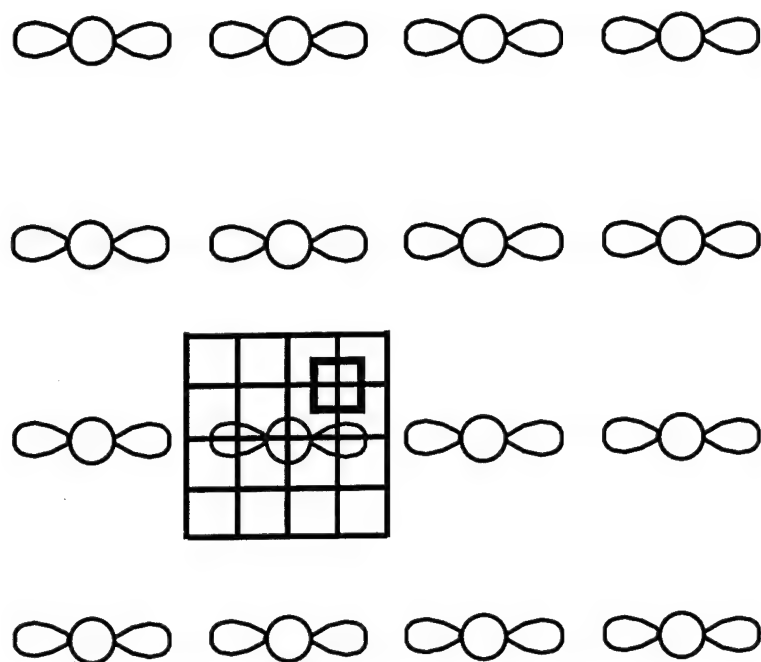
Figure 12. Schematic representation of the 3-layer Si slab employed for the study of the (100)-diamond/(100)-Si interface interaction: (a) top view and (b) side view. The Si atoms of the bottom surface are capped with hydrogen atoms.

hydrogen atoms as in Fig. 12. For the 3-layer silicon slab, the bottom surface Si atoms are capped with hydrogen atoms [43], and the dangling bonds of the top surface Si atoms are exposed to engage in interface interactions.

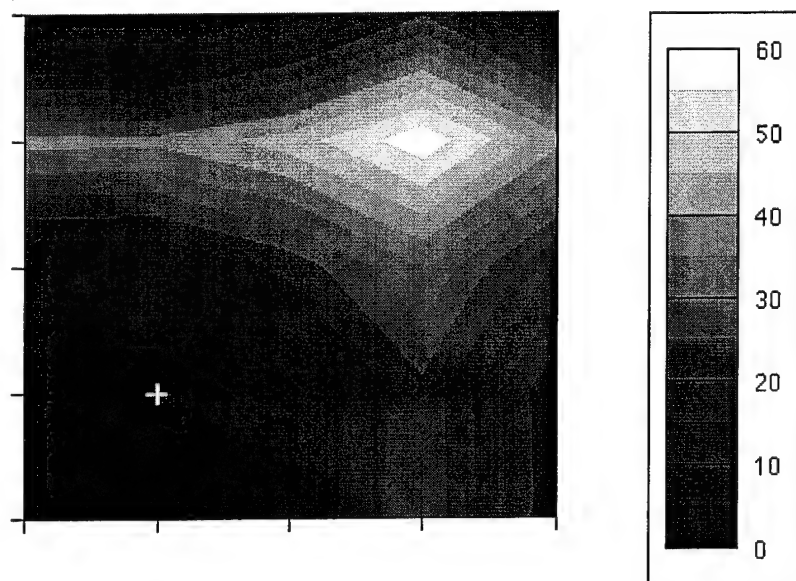
To examine the preferred orientation of the C<sub>7</sub> diamond cluster with respect to the 3-layer silicon slab, we consider three arrangements: parallel, 45°-rotation and perpendicular. The (100) planes containing the two dangling bonds of the Si atoms make 0°, 45° and 90° with respect to those of the carbon atoms in the parallel, 45°-rotation and perpendicular arrangements, respectively. The parallel and perpendicular arrangements correspond to the 3:2-match structure. To determine the relative stabilities and the optimum structures of the three arrangements, we construct an overlayer of the C<sub>7</sub> diamond clusters on the 3-layer silicon slab with the repeat unit cell leading to a (4×4) surface unit cell. The latter is large enough to ensure negligible interactions between adjacent C<sub>7</sub> diamond clusters in the overlayer. On the basis of EHTB electronic band structure calculations, we then calculate the energies of the overlayer/Si-slab system for the parallel, 45°-rotation and perpendicular arrangements as a function of the interface separation and the position of the C<sub>7</sub> diamond cluster within the unit cell. In our calculations, the geometries of the interacting fragments (i.e., the C<sub>7</sub> diamond clusters and the 3-layer Si slab) were kept frozen [43].

For the parallel arrangement, Figure 13a shows mesh points of geometries used to find the optimum position of the C<sub>7</sub> diamond cluster (at an interface separation of 2 Å), Figure 13b the energy contour diagram associated with these mesh point calculations, and Figure 14a the optimum position determined from this search. Figures 14b and 14c show the optimum positions of the C<sub>7</sub> diamond cluster found for the 45°-rotation and perpendicular arrangements in a similar manner. Our calculations as a function of the interface separation show that the interface interaction has a very shallow minimum at an interface separation of around 2.3 Å for the parallel and perpendicular arrangements, but it is repulsive for the 45°-rotation arrangement. The parallel and perpendicular arrangements are similar in stability, and the small stability difference between the two (about 5 kcal/mol in favor of the perpendicular arrangement) is insignificant. However, the parallel and perpendicular arrangements are much more stable than the 45°-rotation arrangement (by about 50 kcal/mol). These results are consistent with the conclusions from our HRTEM, polar Raman and polar XRD studies.

It is of interest to analyze the essence of the interface interactions associated with the parallel, 45°-rotation, and perpendicular arrangements. From the viewpoint of the tetrahedral bonding of a carbon atom in bulk diamond and a silicon atom in bulk silicon, the (100) surface atoms of diamond and Si are considered to possess two sp<sup>3</sup> hybrid orbitals. In the molecular orbital picture these hybrid orbitals are linearly combined to form the n<sub>z</sub> and p<sub>π</sub> orbitals [44] (Fig. 15). The axes of the p<sub>π</sub> orbitals are contained in the (100) surface, and those of the n<sub>z</sub>

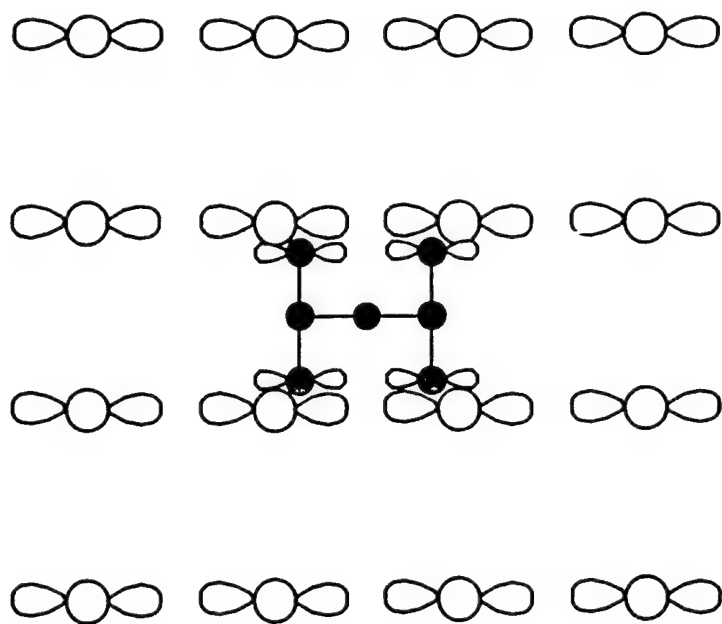


a

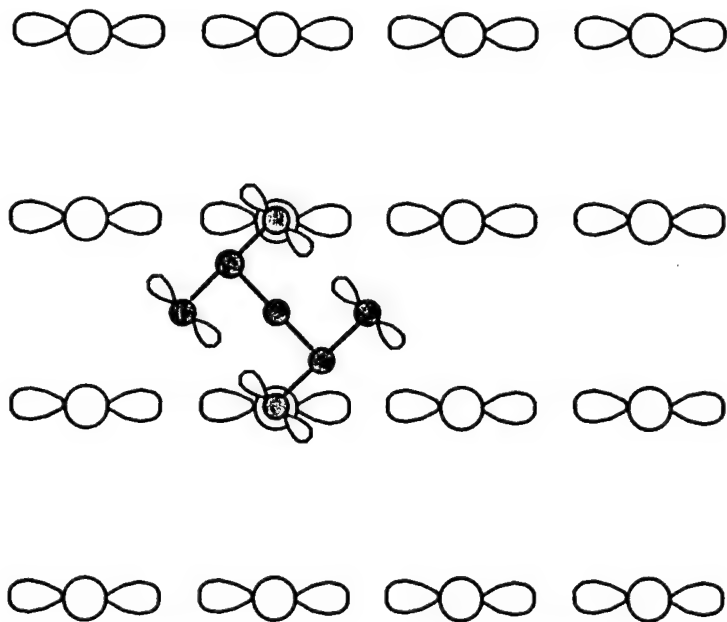


b

Figure 13. (a) Mesh points of the positions considered for the  $C_7$  cluster above the  $(4 \times 4)$  surface unit cell of the 3-layer Si slab in determining the optimum position of the  $C_7$  cluster for the parallel arrangement. The circles represent the Si atoms, and the orbital lobes the dangling bonds. The small square inlaid at the upper right corner defines the fine-mesh points used for a more accurate geometry search. (b) Energy contour diagram associated with the fine-mesh points for the parallel arrangement, where the lowest energy point is indicated by a cross, and the values of the energy contours are given with respect to the minimum energy point.



a



b

Figure 14. Optimum positions of the C<sub>7</sub> cluster calculated for the (a) parallel, (b) 45°-rotation and (c) perpendicular arrangements. The large open and small filled circles represent the Si and C atoms, respectively, and the orbital lobes represent the dangling bonds.

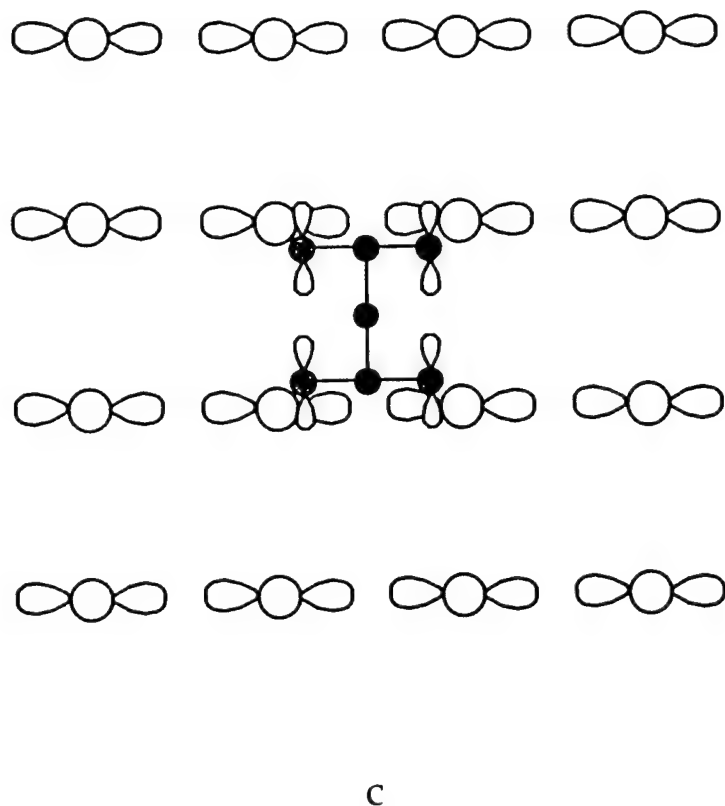


Figure 14. Con't.

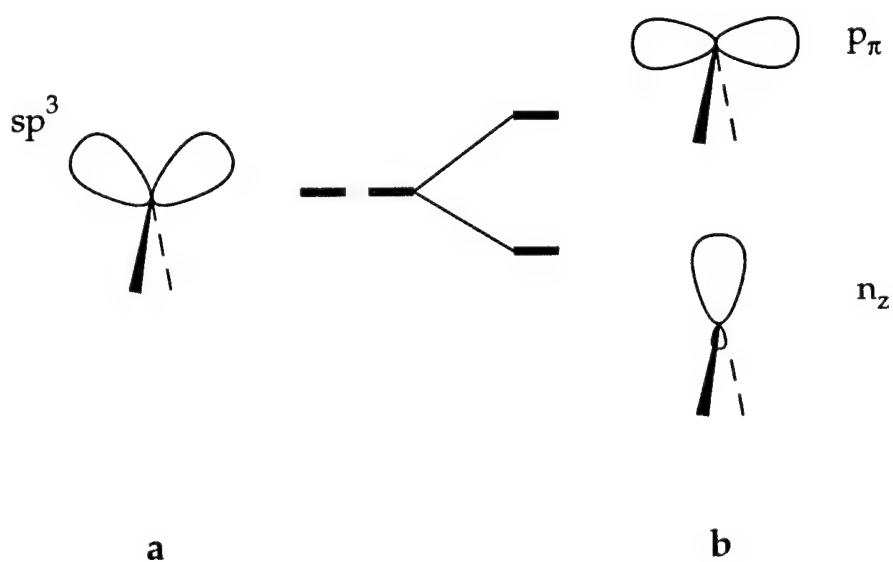


Figure 15. Dangling orbitals of an atom on the (100) surface of the diamond and Si lattices in the bond orbital and molecular orbital representations in (a) and (b), respectively. The  $p_\pi$  and  $n_z$  of the molecular orbital picture are given by the out-of-phase and in-phase combinations of the two  $sp^3$  hybrid orbitals of the bond orbital picture.

orbitals are normal to the surface. The main contributions of the  $n_z$  orbital are the  $p_z$  and  $s$  orbitals. [Here, we follow the convention that the  $z$ -axis is perpendicular to the (100) surface.] Figure 16a presents the projected density of states (PDOS) for the  $p_z$  and  $p_\pi$  orbitals of the four surface carbon atoms of the  $C_7$  diamond cluster. What happens to these PDOS when the diamond cluster interacts with the 3-layer silicon slab is also shown in Fig. 16b for the parallel arrangement: the most significant change the interface interactions bring about lies in the PDOS peak of the  $p_z$  orbitals (around -11.5 eV), which becomes “split” into the lower and higher peaks (around -15.5 eV and -2.5 eV). The split results because the surface atom  $p_z$  orbitals of the diamond cluster establish bonding and antibonding interactions with the surface atom orbitals of the Si substrate. A similar analysis for the perpendicular arrangement reveals the

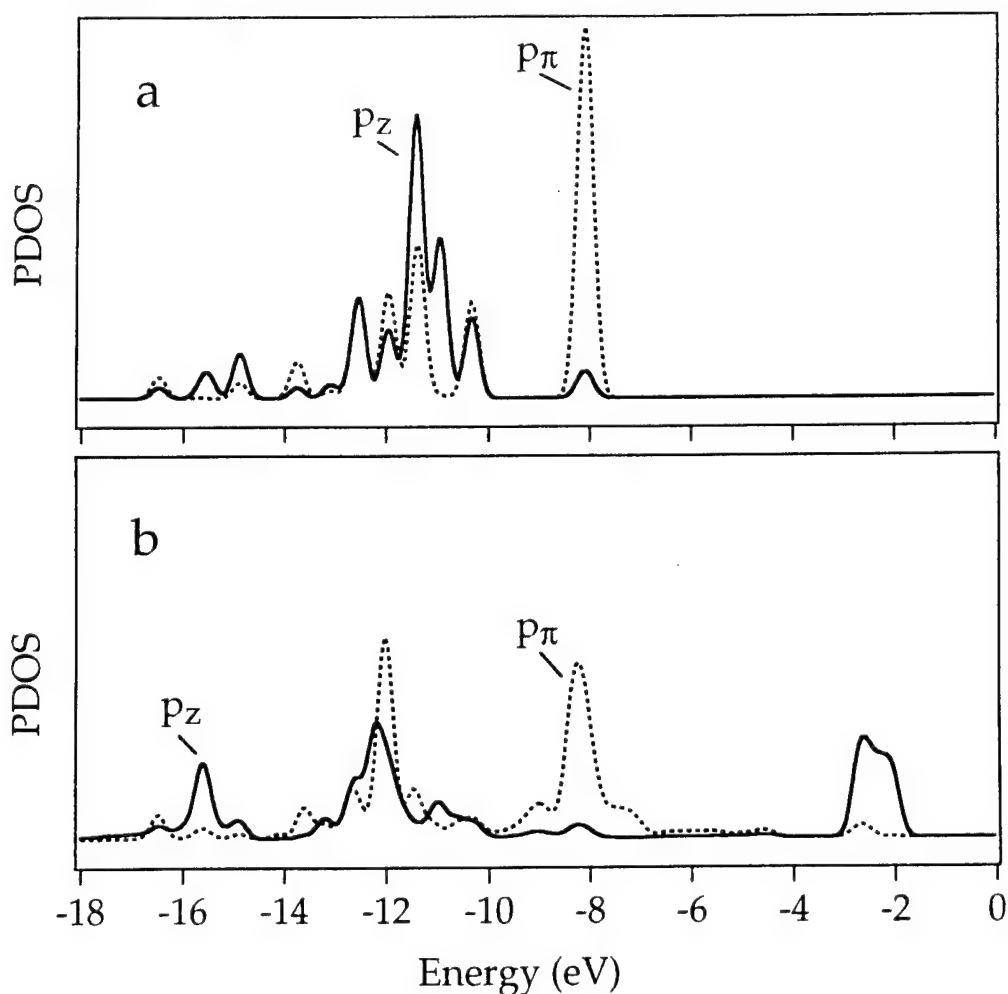


Figure 16. PDOS plots of the  $p_\pi$  (dotted) and  $p_z$  (solid) orbitals calculated for the four bottom surface carbon atoms of the  $C_7$  cluster in the parallel arrangement: (a) before and (b) after interface interaction. The PDOS scales are the same in the two figures but are given in arbitrary units.

same trends. These results indicate that the  $n_z$  orbitals, being perpendicular to the surface, provide good overlap with the surface Si orbitals, so the carbon atom prefers to sit atop the silicon atom. The  $C_7$  diamond cluster used in our model study has four carbon atoms to engage in the interface interactions. The 3:2-match arrangement (i.e., parallel or perpendicular one) can have more carbon atoms atop the silicon atoms than the  $45^\circ$ -rotation arrangement can (4 versus 2). Thus, the 3:2-match arrangement is energetically more favorable than the  $45^\circ$ -rotation arrangement. Use of a larger diamond cluster for our calculations of the interface interactions is unlikely to alter this conclusion, since the  $45^\circ$ -rotation arrangement has a much larger lattice mismatch than the 3:2-match arrangement (7 versus 1.5 %).

Our calculations do not include the elastic deformation of the heteroepitaxial layer, but the results are in qualitative agreement with experiment. It is interesting to note from Verwoerd's study [27,28] that the 3:2-match arrangement becomes energetically favored over the  $45^\circ$ -rotated arrangement when the diamond overlayer is greater than 3 atomic layers. (Since the experimental measurements deal with micrometer layer thicknesses, i.e., thousands of atomic layers, Verwoerd's conclusion is in agreement with experiment.) This implies that as the thickness of the diamond layer increases, the relaxation of the carbon atoms at the interface becomes weaker, probably because the C-C bond is stronger than the C-Si bond.

*Growth on  $Ni_3Si$  and Ni.* The diamond growth on  $Ni_3Si$  is remarkable in that very little graphite is observed. Under similar conditions, the growth on Ni substrates is largely graphitic. To gain insight into these differences, we examine the tendency of the  $Ni_3Si$  and Ni substrates for diamond versus graphite nucleation on the basis of EHTB electronic band calculations. As structural models for the study of their (111) and (100) surfaces, we employ 3- and 4-layers thick substrate slabs, respectively. The (111) surface is especially interesting because both diamond and graphite can be epitaxially matched on this surface. To simulate the beginning stage of diamond and graphite nucleation, we place on these slabs one, two or three  $C_2$  units (i.e.,  $C_2$ ,  $C_4$  or  $C_6$  unit) in orientations that imitate the diamond and graphite structures. Figures 17a and 17b schematically show the (111) and (100) surface atoms in Ni and  $Ni_3Si$ , respectively, where  $(1 \times 2)$  unit cells are drawn in. We used a  $(1 \times 2)$  surface unit cell to place one or two  $C_2$  units, and a  $(1 \times 3)$  surface unit cell to place three  $C_2$  units. As depicted in Figs. 18a-18c, where the filled circles represent the atom, hollow, or bridge positions of the surface, the  $C_2$  units of a unit cell were placed above the surface at a distance  $r$  from the "anchor" carbon of each  $C_2$  (i.e., the one indicated by the dashed line). The anchor carbon atoms were lined up along the x-axis, so that the  $C_2$  units form a carbon-carbon zigzag chain if a unit cell has more than one  $C_2$  unit (e.g.,  $C_4$  and  $C_6$  zigzag chains).

For the simulation of diamond nucleation, we fixed the C-C bond length of  $C_2$  to 1.54 Å, and made the C-C bond non-parallel to the substrate surface. The angle  $\alpha$  of Figure 18a was

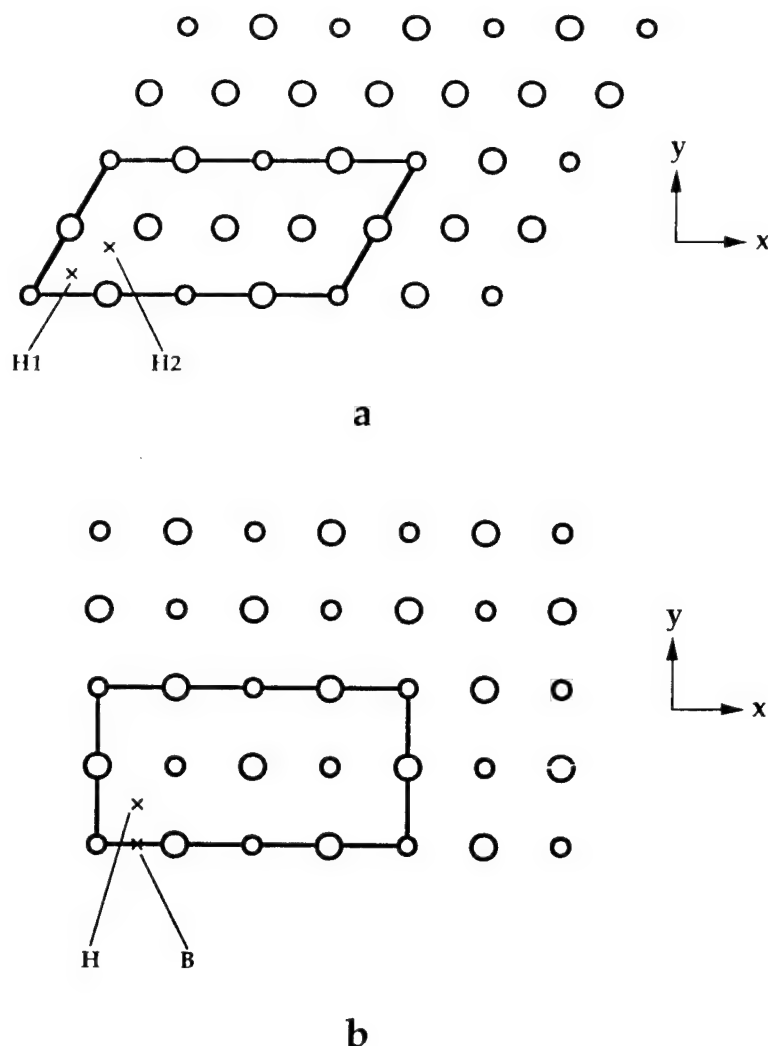
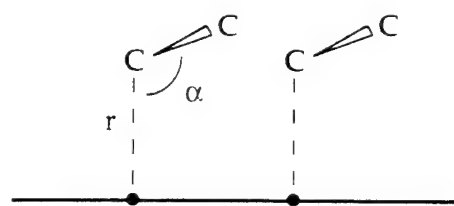
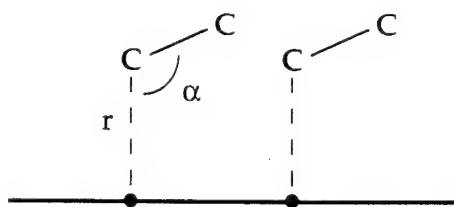


Figure 17. Schematic representation of the atom arrangements on the (111) and (100) surfaces of  $\text{Ni}_3\text{Si}$ : (a) (111) surface and (b) (100) surface. The small and large circles represent the Si and Ni atoms, respectively. These representations are also valid for Ni, for which all the surface atoms are equivalent. For convenience, (1x2) surface unit cells are indicated. The labels H, H1 and H2 refer to hollow sites, and the label B a bridge site.

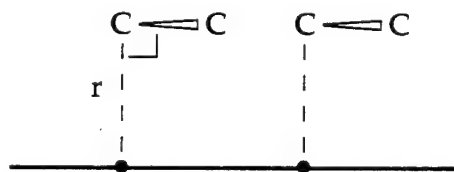
fixed at  $109.47^\circ$  and  $126^\circ$  for the (111) and (100) surfaces, respectively. With respect to the coordinate x-axis (Fig. 17a), the perpendicular plane containing a  $\text{C}_2$  unit was rotated by  $30^\circ$  for the (111) surface (Fig. 18a) and by  $0^\circ$  for the (100) surface (Fig. 18b). For the simulation of graphite nucleation, we fixed the C-C bond length of  $\text{C}_2$  to  $1.415 \text{ \AA}$ , and made the C-C bond parallel to the substrate surface (Fig. 18c). With respect to the coordinate x-axis of Fig. 17b, the perpendicular plane containing a  $\text{C}_2$  unit was rotated by  $30^\circ$  for the (111) and (100) surfaces.



a



b



c

Figure 18. Arrangements of  $C_2$  units on the (111) and (100) surfaces of  $Ni_3Si$  and Ni to simulate (a) diamond nucleation on the (111) surface, (b) diamond nucleation on the (100) surface, and (c) graphite nucleation on the (111) and (100) surfaces. A dashed line is shown from one carbon atom (i.e., "anchor" carbon) of each  $C_2$  to the surface. For simplicity, only two  $C_2$  units (to form a  $C_4$  zigzag chain) are shown. The filled circles on the horizontal line represent the atom, hollow, or bridge positions of the surface.

Results of our EHTB calculations for the  $C_n$ -overlayer/substrate ( $n = 2, 4, 6$ ) systems [34] are summarized in Table II. Both the (111) and (100) surfaces of  $Ni_3Si$  show a strong preference for diamond-nucleation over graphite-nucleation at all positions of the anchor carbon atoms. On the surfaces of Ni, diamond- and graphite-nucleations are equally probable or graphite nucleation is slightly favored, except for the atop positions of the (100) surface where diamond nucleation is slightly favored. These computational results are in general consistent with the experimental findings that the growth on Ni gives rise to a mixture of amorphous carbon and graphite, while that on  $Ni_3Si$  results in diamond particles.

Table I. Energy of the diamond-nucleation arrangement with respect to the graphite-nucleation arrangement on the (111) and (100) surfaces of  $Ni_3Si$  and Ni as calculated for the  $C_n$ -overlayer/substrate ( $n = 2, 4, 6$ ) systems (in kcal/mol per  $C_2$  unit).<sup>a,b</sup>

Overlayer	(111) surface		(100) surface		
	Atop	Hollow <sup>c</sup>	Atop	Hollow	Bridge
$C_2$ on $Ni_3Si$	-18 <sup>d</sup> (-13 <sup>e</sup> )	-18(-8.5)	-50 <sup>d</sup> (-38 <sup>e</sup> )	-38	-28
$C_4$ on $Ni_3Si$	-21	-11	-55	-27	-27
$C_6$ on $Ni_3Si$	-23	-13	-62	-25	-34
$C_2$ on Ni	1.8	4.7(4.7)	-6.1	23	6.9
$C_4$ on Ni	0.1	9.3	-21	28	5.8
$C_6$ on Ni	0.3	5.5	-21	26	4.2

<sup>a</sup> The negative numbers mean that diamond-nucleation is preferred over graphite-nucleation.

<sup>b</sup> The distance  $r$  from the anchor carbon atoms to the surface is chosen such that the bond lengths between the anchor carbon and the surface atoms are 2.0 Å. Thus,  $r = 2.0$  Å for the atop position of the (111) and (100) surfaces, 1.4 Å for the hollow position of the (111) surface, 0.95 Å for the hollow position of the (100) surface, and 1.6 Å for the bridge position of the (100) surface.

<sup>c</sup> The numbers in parentheses refer to the hollow sites H2, and all other numbers to the hollow sites H1.

<sup>d</sup> Atop Si. <sup>e</sup> Atop Ni.

## E. Concluding Remarks

Oriented diamond particles are deposited on (100) silicon and can be textured to provide nearly 100 % alignment with the substrate, although there exists a significant lattice mismatch (34 %). According to our polar Raman, polar XRD and cross-sectional HRTEM studies of the diamond grown on (100) Si surface, the (100)-diamond/(100)-Si interface does not have the 45°-rotation arrangement but the 3:2-match arrangement. In agreement with this finding, our EHTB electronic band structure calculations for a model system show that the interface interaction favors the 3:2-match arrangement (either the parallel or the perpendicular one) over

the 45°-rotation arrangement. In his semi-empirical SCF-MO study Verwoerd reached the same conclusion when the diamond overlayer of his model calculations was made thick enough [27,28].

As a new heteroepitaxial substrate for diamond, we examined diamond growth on Ni<sub>3</sub>Si, because it has a small lattice mismatch and contains silicon to form bonds with carbon. Our experiments with polycrystalline Ni<sub>3</sub>Si show the growth of oriented diamond particles and the lack of graphite formation. In contrast, under the same growth conditions as used for diamond growth on Ni<sub>3</sub>Si, largely graphite was formed on the nickel substrate. Our EHTB calculations for model systems show that both the (111) and (100) surfaces of Ni<sub>3</sub>Si have a strong preference of diamond-nucleation over graphite-nucleation, but this is not the case for the (111) and (100) surfaces of Ni. These computational results are consistent with the experimental findings.

#### F. Acknowledgments

This work was partially supported through the Ballistic Missile Defense Organization/Innovative Science and Technology and the University Research Initiative through the Office of Naval Research. The measurements of Raman spectra by A. Somashekhar are greatly appreciated. Also, we thank Dr. C. T. Liu for the silicide fabrication and Dr. R. C. Glass for polar XRD measurements. M.-H. W. thanks the financial support from the Office of Basic Energy Sciences, Division of Materials Sciences, U. S. Department of Energy, under Grant DE-FG05-86ER45259.

#### G. References

1. S. Koizumi, T. Murakami, T. Inuzuka, and K. Suzuki, *Appl. Phys. Lett.*, **57** (1990) 563.
2. H. Maeda, S. Masuda, K. Kusakabe, and S. Morooka, *Diamond and Related Materials*, **3** (1994) 398.
3. (a) M. Yoshikawa, H. Ishida, A. Ishitani, T. Murakami, S. Koizumi, and T. Inuzuka, *Appl. Phys. Lett.*, **57** (1990) 428.  
(b) M. Yoshikawa, H. Ishida, A. Ishitana, S. Koizumi, and T. Inuzuka, *Appl. Phys. Lett.*, **58** (1991) 1387.
4. A. Argoitia, J. C. Angus, J. S. Ma, L. Wang, P. Pirouz, W. R. L. Lambrecht, *J. Mater. Res.*, **9** (1994) 1849.
5. B. R. Stoner, S. Sahaida, J. P. Bade, P. Southworth, and P.J. Ellis, *J. Mater. Res.*, **8** (1993) 1334.
6. S. D. Wolter, B. R. Stoner, J. T. Glass, P. J. Ellis, D. S. Buhaenko, C. E. Jenkins, and P. Southworth, *Appl. Phys. Lett.*, **62** (1993) 1215.
7. X. Jiang, C.-P. Klages, R. Zachai, M. Hartweg, and H.-J. Füsser, *Appl. Phys. Lett.*, **63** (1993) 3438.
8. B. R. Stoner and J. T. Glass, *Appl. Phys. Lett.*, **60** (1992) 698.
9. B. R. Stoner, G. H. Ma, S. D. Wolter, W. Zhu, Y.-C. Wang, R. F. Davis, and J. T. Glass, *Diamond and Related Materials*, **2** (1993) 142.
10. W. Zhu, X. H. Wang, B. R. Stoner, G. H. M. Ma, H. S. Kong, M. W. H. Braun, and J. T. Glass, *Phys. Rev. B*, **47** (1993) 6529.

11. Y. Sato, H. Fujita, T. Ando, T. Tanaka, and M. Kamo, *Phil. Trans. R. Soc. Lond. A*, **342** (1993) 225.
12. P. C. Yang, W. Zhu, and J. T. Glass, *J. Mater. Res.*, **8** (1993) 1773.
13. P. C. Yang, W. Zhu, and J. T. Glass, in *Proc. Third International Symposium on Diamond Materials*, Honolulu, Eds., J.P. Dismukes, K.V. Ravi, K.E. Spear, B. Lux, and N. Setaka (The Electrochemical Society, 1993) p. 435.
14. P. C. Yang, W. Zhu, and J. T. Glass, *J. Mater. Res.*, **9** (1994) 1063.
15. W. Zhu, P. C. Yang, and J. T. Glass, *Appl. Phys. Lett.*, **63** (1993) 1640.
16. W. Liu, D. A. Tucker, P. C. Yang, and J. T. Glass, to be published.
17. A. Argoitia, J. C. Angus, L. Wang, X. I. Ning, and P. Pirouz, *J. Appl. Phys.*, **73** (1993) 4305.
18. (a) J. C. Angus, Z. Li, M. Sunkara, C. Lee, W. R. L. Lambrecht, and B. Segall, in *Proc. The Third International Symposium on Diamond Materials*, Honolulu, Eds., J. P. Dismukes, K.V. Ravi, K.E. Spear, B. Lux, and N. Setaka (The Electrochemical Society, 1993) p. 128.  
(b) W.R.L. Lambrecht, C. H. Lee, B. Segall, J.C. Angus, Z. Li, and M. Sunkara, *Nature*, **364** (1993) 607.
19. K. Larsson, J.-O. Carlsson, and S. Lunell, *Journal of Physical Chemistry*, **98** (1994) 5019.
20. B. R. Stoner, B. E. Williams, S.D. Wolter, K. Nishimura, and J.T. Glass, *J. Mater. Res.*, **7** (1992) 257.
21. B. R. Stoner, G.-H.M. Ma, S. D. Wolter, and J. T. Glass, *Phys. Rev. B*, **45** (1992) 11067.
22. A. van der Drift, *Philips Res. Rep.*, **22** (1967) 267.
23. D. N. Belton and S. J. Schmieg, *J. Appl. Phys.*, **66** (1989) 4223.
24. D. N. Belton and S. J. Schmieg, *J. Vac. Sci. Technol. A*, **8** (1990) 2353.
25. W. S. Verwoerd and K. Weimer, *Surf. Coat. Technol.*, **47** (1991) 578.
26. W. S. Verwoerd, *Diamond and Related Materials*, **1** (1992) 195.
27. W. S. Verwoerd, *Surface Sci.*, **304** (1994) 24.
28. W. S. Verwoerd, *Diamond and Related Materials*, **3** (1994) 457.
29. S. C. Erwin, M. R. Pederson, and W. E. Pickett, *Phys. Rev. B*, **41** (1990) 10437.
30. S. C. Erwin and W. E. Pickett, in *Proc. Atomic scale calculations of structure in materials*, San Francisco, Eds., M.A. Schluter and M.S. Daw (Materials Research Society, 1990) p. 59.
31. S. C. Erwin and W.E. Pickett, *Surf. Coat. Technol.*, **47** (1991) 487.
32. W. E. Pickett and S. C. Erwin, *Superlattices and Microstructures*, **7** (1990) 335.
33. W. E. Pickett and S. C. Erwin, in *Proc. Diamond, Silicon Carbide and Related Wide-Bandgap Semiconductors*, Boston, Eds., J. T. Glass, R. F. Messier, and N. Fujimori (Materials Research Society, 1990) p. 35.
34. W. E. Pickett and S. C. Erwin, *Phys. Rev. B*, **41** (1990) 9756.
35. W. E. Pickett, M. R. Pederson, K. A. Jackson, and S. C. Erwin, in *Proc. Wide Band Gap Semiconductors Symposium*, Boston, Eds., T.D. Moustakas, J. I. Pankove, and Y. Hamakawa (Materials Research Society, 1992) p. 3.
36. M.-H. Whangbo and R. Hoffman, *Journal of the American Chemical Society*, **100** (1978) 6093.
37. R. Kohl, C. Wild, N. Herres, P. Koidl, B. R. Stoner, and J. T. Glass, *Appl. Phys. Lett.*, **63** (1993) 1792.
38. C. Wild, N. Herres, and P. Koidl, *J. App. Phys.*, **68** (1990) 973.
39. C. Wild, P. Koidl, N. Herres, W. Müller-Sebert, and T. Eckermann, in *Proc. Diamond Materials*, Pennington, Eds., A. J. Purdes, B. S. Meyerson, J.C. Angus, K. E. Spear, R. F. Davis, and M. Yoder (The Electrochemical Society, 1991) p. 224.
40. X. Jiang, R. Six, C.-P. Klages, R. Zachai, M. Hartweg, and H.-J. Füsser, in *Proc. Third International Conference on the New Diamond Science and Technology*, Heidelberg, Eds., P.K. Bachmann, A.T. Collins, and M. Seal (Elsevier, 1993) p. 407.
41. W. Hayes and R. Loudon, *Scattering of Light by Crystals* (Wiley, 1978).

42. D. S. Knight and W. B. White, *J. Mater. Res.*, **4** (1989) 385.
43. The atomic parameters of C, Si, Ni and H employed in our EHTB calculations are as follows: the valence shell ionization potentials  $H_{\mu\mu}$  (eV) of the Slater type orbitals (STO's)  $\chi_{\mu}$  are -21.4 ( $C_{2s}$ ), -11.4 ( $C_{2p}$ ), -17.3 ( $Si_{3s}$ ), -9.2 ( $Si_{3p}$ ), -9.9 ( $Ni_{3d}$ ), -7.8 ( $Ni_{4s}$ ), -3.7 ( $Ni_{4p}$ ), -13.6 ( $H_{1s}$ , used to cap the C dangling bonds), and -20.0 ( $H_{1s}$ , used to cap Si dangling bonds). The exponents ( $\xi$  and  $\xi'$ ) and the mixing coefficients ( $c$  and  $c'$ ) of two STO's  $\chi_{\mu}$  and  $\chi_{\mu}'$  to form double a zeta orbital ( $c \chi_{\mu} + c' \chi_{\mu}'$ ) are: ( $\xi, c, \xi', c'$ ) = (1.831, 0.7931, 1.152, 0.2739) for  $C_{2s}$ , (2.730, 0.2595, 1.257, 0.8026) for  $C_{2p}$ , (2.059, 0.5843, 1.297, 0.5187) for  $Si_{3s}$ , (1.819, 0.4216, 1.065, 0.6577) for  $Si_{3p}$ , (5.75, 0.5683, 2.00, 0.6292) for  $Ni_{3d}$ . The single zeta STO's used are:  $\xi = 1.3$  for  $H_{1s}$  (for capping the C dangling bonds), 1.1 for  $H_{1s}$  (for capping the Si dangling bonds), 2.1 for  $Ni_{4s}$  and  $Ni_{4p}$ . For  $Ni_3Si$ , Si was represented by the single zeta STO's with  $\xi = 1.624$  for  $Si_{3s}$  and 1.428 for  $Si_{3p}$ .
44. T. A. Albright, J. K. Burdett, and M.-H. Whangbo, *Orbital Interactions in Chemistry* (Wiley, 1985).

### III. Distribution List

Mr. Max Yoder Office of Naval Research Electronics Division, Code: 312 Ballston Tower One 800 N. Quincy Street Arlington, VA 22217-5660	3
Administrative Contracting Officer Office of Naval Research Regional Office Atlanta 101 Marietta Tower, Suite 2805 101 Marietta Street Atlanta, GA 30332-0490	1
Director, Naval Research Laboratory ATTN: Code 2627 Washington, DC 20375	1
Defense Technical Information Center Bldg. 5, Cameron Station Alexandria, VA 22314	2